Geochemistry, Geophysics, Geosystems

Supporting Information for

Experimental investigation of the pressure of crystallization of $Ca(OH)_2$: Implications for the reactive-cracking process

S. Lambart[1,2], H. M. Savage[1], B. G. Robinson[1] and P. B. Kelemen[1]

1 Lamont-Doherty Earth Observatory, Columbia University, Palisades, NY 10964, USA.

2 University of Utah, Geology and Geophysics, Salt Lake City, UT 84112, USA.

Contents of this file

Texts S1 to S6

Figures S1 to S5

Table S1

Additional Supporting Information (Files uploaded separately)

Tables S2 and S3

Introduction

The supporting information complements the main text by:

• Providing additional detailed descriptions (in Text sections S1 to S6 and in Figs. S1 to S5)

• Providing the complete data set of experimental conditions and results (Tables S1-S3)

Text S1. Theoretical volume changes, maximal *P'*, and final reaction progress and porosities in the experimental products

This section presents the data and equations used to calculate the volume changes of the solid and the total volume changes during full hydration of CaO and full carbonation of forsterite, the maximal pressure of crystallization for CaO hydration and forsterite carbonation, and the %$Ca(OH)_2$ and porosity in the final products of our experiments.

Theoretical volume changes and pressure of crystallization:

Table S1. Density (ρ), molar masses (M), reactions, percentage of solid volume (%ΔVs) and total volume (%ΔVr) change, Gibbs free energy of reactions (ΔGr) and calculated maximal pressure of crystallization (*P'*) for full CaO hydration and forsterite carbonation.

	ρ ($g.cm^{-3}$)	M ($g.mol^{-1}$)	Hydration/ carbonation reaction	%ΔVs	%ΔVr	ΔGr ($kJ.mol^{-1}$)	P'_{max} = - ΔGr/ΔVs (GPa)
CaO	3.34[1]	56.079	$CaO + H_2O \rightarrow Ca(OH)_2$	+96%	-5.4%	-57[7]	3.5
H_2O	1[2]	18.015					
$Ca(OH)_2$	2.25[3]	74.094					
Mg_2SiO_4	3.22[4]	140.692	$Mg_2SiO_4 + 2CO_2 \rightarrow 2MgCO_3 + SiO_2$	+84%	-9.2%	-70[8]	1.9
CO_2	1.977[5]	44.009					
SiO2	2.65[1]	60.084					
MgCO3	2.96[6]	84.313					

[1] Haynes, 2011; [2] at 1 bar and 25°C; [3] Taylor, 1997; [4] Kumazawa and Anderson, 1969; [5] at 1 bar and 0°C; [6] Kornprobst and Plank, 2013; [7] calculated from the standard Gibbs energy of formation ;[8] at 1 bar and 25°C (Kelemen and Hirth, 2012).

Percent of volume changes ΔVs and ΔVr for CaO hydration are:

$$\%\Delta V_S = \frac{M_{Ca(OH)_2}/\rho_{Ca(OH)_2} - M_{CaO}/\rho_{CaO}}{M_{CaO}/\rho_{CaO}} * 100 \qquad \text{(S1)}$$

$$\%\Delta V_R = \frac{M_{Ca(OH)_2}/\rho_{Ca(OH)_2} - \left(M_{CaO}/\rho_{CaO} + M_{H_2O}/\rho_{H_2O}\right)}{M_{CaO}/\rho_{CaO} + M_{H_2O}/\rho_{H_2O}} * 100 \qquad \text{(S2)}$$

The absolute solid volume change during hydration of 1 mole of CaO is:

$$\Delta \boldsymbol{V_S} = {\boldsymbol{M_{Ca(OH)_2}}}/{\boldsymbol{\rho_{Ca(OH)_2}}} - {\boldsymbol{M_{CaO}}}/{\boldsymbol{\rho_{CaO}}} = 16.14 \text{ cm}^3.\text{mol}^{-1} \quad \text{(S3)}$$

Percent of volume changes ΔVs and ΔVr for forsterite carbonation are:

$$\%\Delta \boldsymbol{V_S} = \frac{\boldsymbol{2_*}{\boldsymbol{M_{MgCO_3}}}/{\boldsymbol{\rho_{MgCO_3}}} + {\boldsymbol{M_{SiO_2}}}/{\boldsymbol{\rho_{SiO_2}}} - {\boldsymbol{M_{Mg_2SiO_4}}}/{\boldsymbol{\rho_{Mg_2SiO_4}}}}{{\boldsymbol{M_{Mg_2SiO_4}}}/{\boldsymbol{\rho_{Mg_2SiO_4}}}} * \boldsymbol{100} \quad \text{(S4)}$$

$$\%\Delta \boldsymbol{V_R} = \frac{\boldsymbol{2_*}{\boldsymbol{M_{MgCO_3}}}/{\boldsymbol{\rho_{MgCO_3}}} + {\boldsymbol{M_{SiO_2}}}/{\boldsymbol{\rho_{SiO_2}}} - {\boldsymbol{M_{Mg_2SiO_4}}}/{\boldsymbol{\rho_{Mg_2SiO_4}}} - \boldsymbol{2_*}{\boldsymbol{M_{CO_2}}}/{\boldsymbol{\rho_{CO_2}}}}{{\boldsymbol{M_{Mg_2SiO_4}}}/{\boldsymbol{\rho_{Mg_2SiO_4}}} + \boldsymbol{2_*}{\boldsymbol{M_{CO_2}}}/{\boldsymbol{\rho_{CO_2}}}} * \boldsymbol{100} \quad \text{(S5)}$$

The absolute solid volume change for the full carbonation of one mole of forsterite is:

$$\Delta \boldsymbol{V_S} = \boldsymbol{2} * {\boldsymbol{M_{MgCO_3}}}/{\boldsymbol{\rho_{MgCO_3}}} + {\boldsymbol{M_{SiO_2}}}/{\boldsymbol{\rho_{SiO_2}}} - {\boldsymbol{M_{Mg_2SiO_4}}}/{\boldsymbol{\rho_{Mg_2SiO_4}}} = 36.35 \text{ cm}^3.\text{mol}^{-1}. \quad \text{(S6)}$$

Experimental products:

The % $Ca(OH)_2$ in the final product, the final bulk porosity $\Phi_f(bulk)$ and the porosity of the portlandite $\Phi_f(Ca(OH)_2)$ were calculated at the end of each experiments such as:

$$\%Ca(OH)_2 = \frac{m_f - m_0}{m_0} \times \frac{M_{CaO}}{M_{Ca(OH)_2} - M_{CaO}} \times 100 \quad \text{(S7)},$$

$$\Phi_f(bulk) = 1 - \frac{m_f}{\frac{\%Ca(OH)_2}{100} \times d_{Ca(OH)_2} + \left(1 - \frac{\%Ca(OH)_2}{100}\right) \times d_{CaO}} \times \frac{1}{V_f} \quad \text{(S8)}$$

Assuming that the porosity of unreacted CaO stays unchanged during the experiment, we can write:

$$\Phi_f(Ca(OH)_2) = \frac{\Phi_f(bulk) - \left(1 - \frac{\%Ca(OH)_2}{100}\right) \times \Phi_0}{\frac{\%Ca(OH)_2}{100}} \quad \text{(S9)},$$

with m_0 the initial mass of the cylinder, m_f *and* V_f the mass and the volume of the dry cylinder at the end of the experiment, and $M_{Ca(OH)_2}$ and M_{CaO} the molar masses. Precisions of the final length and weight measurements are ± 0.01 cm and ± 0.05 g (Tables 1 and

S2). Error estimates for final measurements are higher than for initial measurements to take into account the potential loss of materials during the extraction from the die. Error propagation has been used to estimate the precision of the $Ca(OH)_2$ proportion and Φ, as reported in Tables 1 and S2. Note that for the three experiments showing evidence of continuing reaction in the furnace (runs #12 and #7 in Table 1 and run # H1 in Table S2), the reaction extent and porosities were calculated using the wet weight of the cylinder and the volume of the cylinder measured just after the experiments (before the drying step). Consequently, reaction extents are overestimated and final porosities are underestimated for these experiments. Calculated values are reported in Tables 1 and S2 but not used in the discussion.

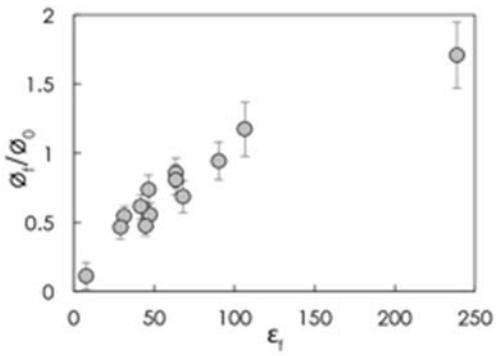

Figure S1. Φ_f/Φ_0 as a function of ε_f for series 1 and 2 experiments with a final extent of reaction higher than 80%.

Figure S1 presents the ratio between the final and the initial porosity, Φ_f/Φ_0, as a function of the final volumetric strain, ε_f, for all experiments in which the final reaction extent was more than 80% (Tables 1 and S2). We observed a large range of variation for Φ_f/Φ_0 from –81% to +69% ($\varnothing_f$ varies from 5% to 63%).

Text S2. Effect of Decarbonation Time

Previous experiments performed on CaO powder suggest that the reactivity of the material decreases with increasing temperature of preparation (above the minimal temperature of calcination of 848°Cat 1atm) due to the sintering of the CaO particles (e.g., Borgwardt, 1989; Miller, 1960; Shin et al., 2009). By choosing a calcination temperature close to the minimal decarbonation temperature, we limit CaO sintering and increase its reactivity. Moreover, the reactivity of CaO is also a function of the decarbonation time. Enough time must be allowed for heat to transfer to the inside of $CaCO_3$ particles and for carbon dioxide gas to be exhausted, but it is also desirable that the calcination time should be as short as possible. Shin et al. (2009) suggested an optimal decarbonation time of 2 hours for similar starting material and conditions. To test this hypothesis, we ran a series of experiments with a constant, small axial load (0.11 MPa), using samples prepared with the first decarbonation step from 2 to 48 hours. Experimental conditions and summary of

the results are presented in Table 1 in the main text (for 2 hours decarbonation step) and Table S2 (for longer decarbonation step).

Figure S2 illustrates the evolution of the volumetric strain as a function of time for nine experiments performed with an axial load of 0.11 MPa, with first decarbonation step durations of 2, 3, 15, 24 and 48 hours at 850°C. Starting materials prepared with the shortest baking time (2 hours; solid lines in Fig. S2) show the highest volumetric strain at a given time, confirming that the reactivity of CaO with water decreases with the duration of decarbonation (Shin et al., 2009). However, we also observed a significant scatter even for experiments performed at the same conditions (i.e. same decarbonation time, axial load and temperature). For instance, the volumetric strain varies between 10 and 30% after one hour for starting materials prepared with a 2 hour decarbonation step, demonstrating that other parameters affect the reactivity of the material. The scatter may be due to a combination of the size of the initial cylinder, the initial porosity, variable lubrication between the sample cylinder and the steel die, and perhaps the amount of impurities in the starting material. In the main text, only experiments performed on cylinders prepared with a 2 hour decarbonation step are presented.

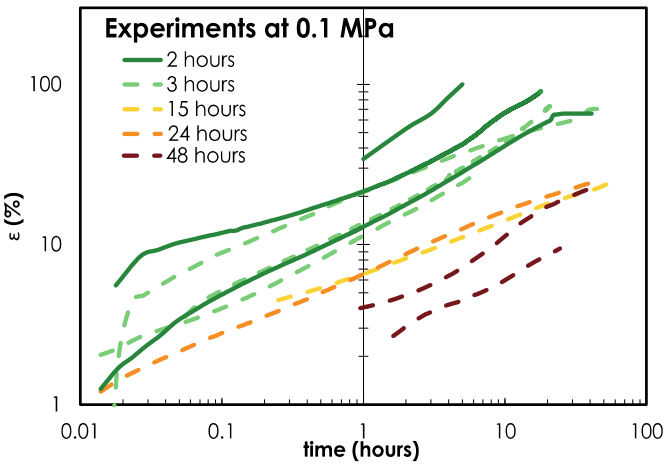

Figure S2. Volumetric strain as a function of time, in response to a uniaxial load of 0.1 MPa for different durations of the decarbonation step. All the experiments were performed at room temperature.

Text S3. Negligible effect of the gravity on the capillarity raise.

The flux Q, through an area a, into a porous body is:

$$Q = \frac{\dot{V}}{a} = \frac{\phi a \dot{h}}{a} = \frac{K}{\eta}\left(\frac{-P_c}{h} - \rho g \sin \Psi\right) \qquad \text{(S10)}$$

with ϕ, the porosity, h = height of rise, K = permeability, η = viscosity of the liquid, ρ = density of liquid, g = gravitational acceleration, and ψ (= π/2) is the angle with respect to horizontal (here $\Psi = \pi/2$) ; P_c = the capillary pressure,

$$-P_c = \frac{2\cos\theta\cdot\gamma}{R_c} \quad \text{(S11)}$$

where θ is the wettability, γ the surface tension and R_c the radius of the pores (e.g., Selker et al., 2007).

Equation (S10) can be simplified as:

$$h\dot{h} + \left(\frac{K\rho g}{\eta\Phi}\right)h = \frac{-KP_c}{\eta\Phi} \quad \text{(S10A)}$$

Defining $A = \frac{K\rho g}{\eta\Phi}$ and $A = \frac{-KP_c}{\eta\Phi}$, we can write (S10A) as:

$$h\dot{h} + Ah = B \quad \text{(S12)}$$

Rearranging equation (S12),

$$\dot{h} = \frac{B-Ah}{h} \qquad \text{(S13).}$$

To assess the importance of gravity for a sample of height h_f, we compared the rates of rise with and without gravity at the point where the liquid reaches the top of the sample (where the gravitational effect is largest).

From equation (S13), the rate of rise at the top of the sample is:

$$\dot{h_1} = \frac{B-Ah_f}{h_f} \qquad \text{(S13A).}$$

While, if we neglect gravity (i.e. $A = 0$):

$$\dot{h_2} = \frac{B}{h_f} \qquad \text{(S13B).}$$

We can define δ as:

$$\delta = 1 - \frac{\dot{h_1}}{\dot{h_2}} = \frac{\rho g h_f}{-P_c} \qquad \text{(S14).}$$

δ varies from 0 to 1 with 0 corresponding to no gravitational effect and 1 with a gravitational effect higher than the pressure of capillarity.

Using equation (S11) we can estimate the maximal radius of the pores for various values of δ. For a 6 cm high cylinder (the tallest cylinder obtained in our experiments, Table 1) and $\gamma = 77.8$ mN.m^{-1} (e.g., Weisbrod et al., 2002), we obtain R_c = 2.5µm for $\delta = 1\%$, R_c = 12.4µm for $\delta = 5\%$ and R_c = 25µm for $\delta = 10\%$.

The diameter of the $Ca(OH)_2$ grains is between 10 and 20µm. Assuming spherical grains,

we can estimate the number of grains, n, in the final cylinder:

$$n = \frac{3}{4}\frac{(1-\Phi)V_c}{\pi(D/2)^3} \qquad \text{(S15)}$$

with V_c the volume of the cylinder and D, the diameter of the grain.

Then, assuming the number of grains is equal to the number of pores and considering spherical pores, we can estimate the radius of the pores R_c:

$$R_c = \sqrt[3]{\frac{3\Phi V_c}{4\pi n}} \qquad \text{(S16).}$$

Considering a 6cm cylinder and a final porosity $\Phi = 0.6$ (run#3 in Table 1), R_c varies between 5 and 10µm. Hence the difference between the rate of the rise with and without the gravitational effect is likely to be less than 5% when the water reaches the top of the cylinder. Note that we considered the case where the gravitational effect would be the largest (run #3, Table 1). A smaller cylinder and a lower porosity would have an even smaller gravitational effect.

Text S4. Volumetric strain and sorptivity

Comparing the evolution of the volumetric strain with time (eq. 3 in the main text) and the equation of Philip (1957) for infiltration in a porous media by capillarity (eq. 7 in the main text), we suggested that the volumetric strain, ε, is proportional to the water infiltration, I. Moreover, based on the analysis presented above, we consider that the gravitational effect is negligible. To further test this assumption, we compared the strains measured in our experiments with the strain calculated using equation (8) in the main text, which we can rewrite:

$$\mathcal{E} = \frac{S_1}{h_0}\sqrt{t} \qquad \text{(S17),}$$

with $S_1 = k_3 S$.

Best-fit values for S_1 were calculated by minimizing the sum of the squares of the difference between the experimental and model values. Figure S3a compares the calculated and experimental strains and Figure S3b illustrates S_1 as a function of the applied load σ. S1 decreases with increasing stress to the power 1 to 1.2, and increases with increasing T. While S_1 is not a direct measure of the sorptivity, the good fit between our experimental data and equation (S10) is consistent with our assumption that water

infiltration in our experiments was primarily driven by capillary flow.

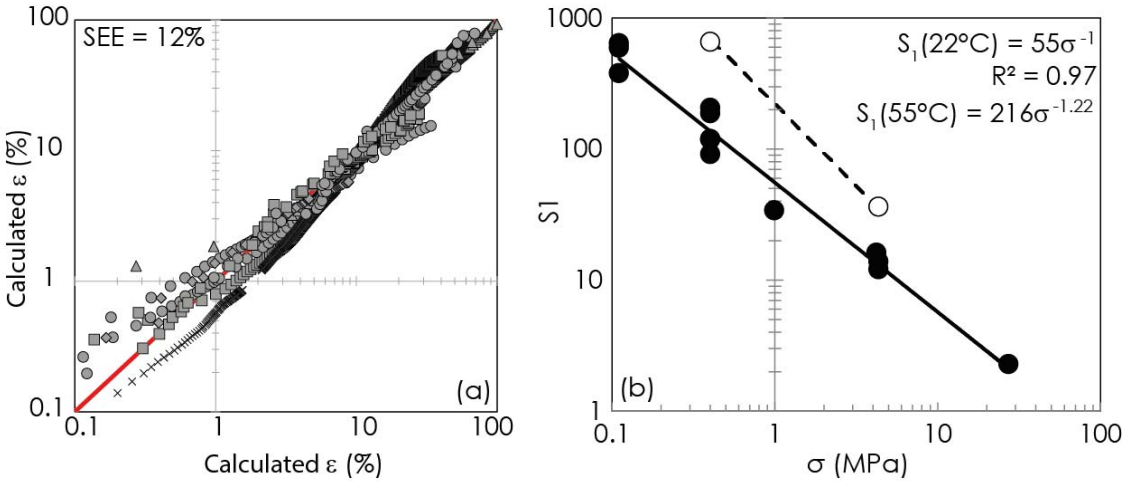

Figure S3. (a) Comparison between measured and calculated strains using equation S17. The red line is the 1:1 line. The average standard error estimate on ε is 12%, relative. Triangles are experiments performed with σ = 0.1 MPa, circles: σ = 0.4 MPa, crosses: σ = 1 MPa, squares: σ = 4.2 MPa, and diamonds: σ = 27.2 MPa. (b) S_1 as a function of σ for experiments at 22°C (filled circles) and 55°C (open circles). Equations are the best-fit lines and R^2 is the correlation coefficient for experiments at 22°C.

Note that in this analysis, S is assumed as a constant with time. However, because the porosity is changing, S is also a function of time. In the capillary model, where the porous medium is assumed to be a bundle of capillary tubes, the permeability can be described as (Dullien, 1992; Masoodi et al., 2010):

$$K = \frac{1}{8} \cdot \Phi_0 \cdot {R_c}^2 \qquad \text{(S18)}.$$

For a uniform isotropic and random material, the volume fraction of a particular phase is equivalent to its area fraction observed on a plane section[14]. Hence,

$$\Phi = n\pi {R_c}^2 \qquad \text{(S19)},$$

with *n*, the number of pores per unit area of the porous medium.

Combining equations (S18) and (S19) with the equation of the sorptivity (eq. 9 in the main text), we obtain:

$$S = \sqrt{\frac{\gamma \cos\theta \cdot \Phi^{0.5}}{2\eta \cdot (n\pi)^{0.5}}} \qquad \text{(S20)}.$$

As a first approximation we can consider θ, γ and η constant during the experiment and Φ as a linear function of the time (t_i):

$$\Phi = \Phi_0 + \alpha t_i \quad \text{(S21)},$$

$$\text{with } \alpha = \frac{\phi_{bulk} - \Phi_0}{t} \qquad \text{(S21A)},$$

where Φ_{bulk} is the porosity of the cylinder at the end of the experiment and *t*, the duration

of the experiment (Table 1). Hence, we can write:

$$S = C \cdot (\Phi_0 + \alpha t_i)^{0.25} \text{ and } C = \sqrt{\frac{\gamma \cos\theta}{2\eta \cdot (n\pi)^{0.5}}} \quad \text{(S22)}.$$

By taking into account the evolution of the porosity with time, equation (S17) can explain 96% of the experimental variance, and SEE is still 12%, suggesting that the change of porosity with time does not significantly affect the strain evolution.

Text S5. Compaction of wet portlandite

One possible explanation for the decrease of final porosity with increasing the axial load (Figure 4 in the main text) might be that the decrease is due to compaction of CaO and/or $Ca(OH)_2$. To test this hypothesis, we performed a compaction experiment on wet portlandite with an axial load of 4.2 MPa, with results shown in Figure S4. To prepare the portlandite cylinder, we baked $CaCO_3$ powder at 850°C for 2 hours and cooled the powder under vacuum in the same condition than for hydration experiments. The powder was then submerged in water. After 30 min, the powder formed a deposit in the bottom of the beaker; we removed most of the water and let the rest evaporate at room temperature. The portlandite powder was then cold-pressed at the same conditions than the CaO powder. The initial porosity of the portlandite cylinder was 41 ± 0.7%. The sample was then saturated in water by submerging the cylinder in a beaker of water and placing the beaker under vacuum for 20 min. The sample was then inserted in the die covered with the same grease as in hydration experiments. After seven days, the volumetric strain was ~1%, far too small to account for the difference in strain between the 0.1 and 4.2 MPa hydration experiments. We infer that compaction processes differ in experiments involving reaction of CaO with H_2O, probably due to rapid consumption of pore space during dissolution of CaO and precipitation of $Ca(OH)_2$.

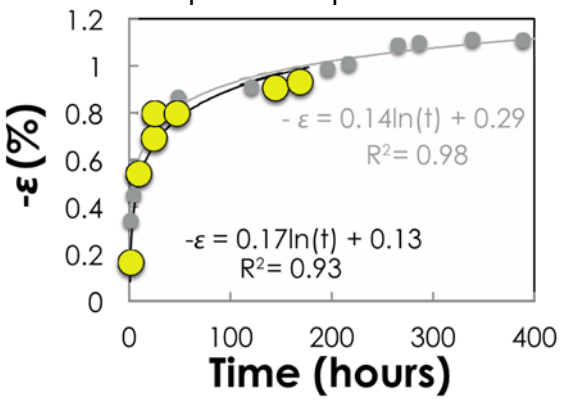

Figure S4. Compaction creep curve for a water-saturated cylinder of portlandite with an applied stress of 4.2 MPa at room temperature (yellow circles) compared with Zhang et al.'s results (2002) on wet calcite (grey circles) for an applied stress of 4 MPa. The solid curves are the best-fits.

Text S6. Estimation of the activation energy, E_a.

Figure S5 shows the strain rate as function of inverse temperature for various values of the strain. Assuming that the strain rate is directly proportional to the reaction rate, the slope of the line in this plot is equal to $-E_a/R$, with E_a, the activation energy for CaO hydration and R the gas constant. Based on Figure S5, we find E_a equal to 66 ± 16 kJ/mol.

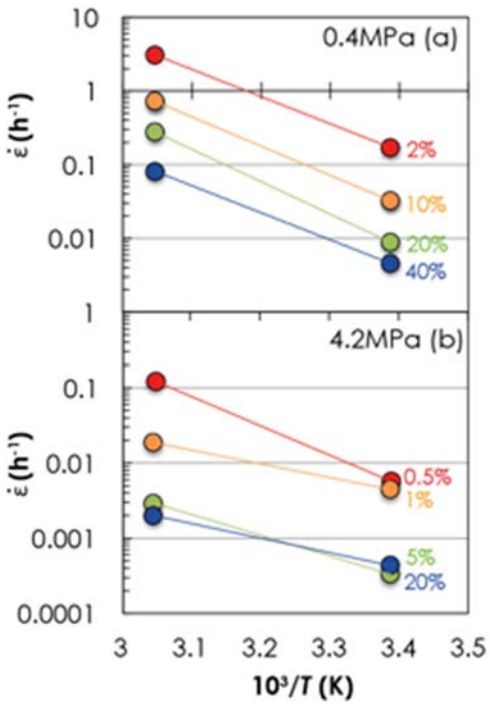

Figure S5. Strain rate as a function of inverse temperature for experiments performed at 0.4 MPa and 2%, 10%, 20% and 40% strain **(a)** and for experiments performed at 4.32 MPa and 0.5, 1%, 5% and 20% strain **(b).**